Acta Neuropathol (2005) 109: 467–474
DOI 10.1007/s00401-005-0985-9

REGULAR PAPER

**Masahiko Iwakiri · Katsuyoshi Mizukami
Milos D. Ikonomovic · Masanori Ishikawa
Shin Hidaka · Eric E. Abrahamson
Steven T. DeKosky · Takashi Asada**

Changes in hippocampal $GABA_BR1$ subunit expression in Alzheimer's patients: association with Braak staging

Received: 12 October 2004 / Revised: 30 December 2004 / Accepted: 3 January 2005 / Published online: 10 March 2005

Abstract Alterations in the γ-aminobutyric acid (GABA) neurotransmitter and receptor systems may contribute to vulnerability of hippocampal pyramidal neurons in Alzheimer's disease (AD). The present study examined the immunohistochemical localization and distribution of $GABA_B$ receptor R1 protein (GBR1) in the hippocampus of 16 aged subjects with a range of neurofibrillary tangle (NFT) pathology as defined by Braak staging (I–VI). GBR1 immunoreactivity (IR) was localized to the soma and processes of hippocampal pyramidal cells and some non-pyramidal interneurons. In control subjects (Braak I/II), the intensity of neuronal GBR1 immunostaining differed among hippocampal fields, being most prominent in the CA4 and CA3/2 fields, moderate in the CA1 field, and very light in the dentate gyrus. AD cases with moderate NFT pathology (Braak III/IV) were characterized by increased GBR1-IR, particularly in the CA4 and CA3/2 fields. In the CA1 field of the majority of AD cases, the numbers of GBR1-IR neurons were significantly reduced, despite the presence of Nissl-labeled neurons in this region. These data indicate that GBR1 expression changes with the progression of NFT in AD hippocampus. At the onset of hippocampal pathology, increased or stable expression of GBR1 could contribute to neuronal resistance to the disease process. Advanced hippocampal pathology appears to be associated with decreased neuronal GBR1 staining in the CA1 region, which precedes neuronal cell death. Thus, changes in hippocampal GBR1 may reflect alterations in the balance between excitatory and inhibitory neurotransmitter systems, which likely contributes to dysfunction of hippocampal circuitry in AD.

Keywords Alzheimer's disease · $GABA_B$ receptor · Hippocampus · Neuronal degeneration · Neurofibrillary tangles

M. Iwakiri · K. Mizukami (✉) · M. Ishikawa
S. Hidaka · T. Asada
Department of Psychiatry, Institute of Clinical Medicine, University of Tsukuba, 1-1-1 Tennodai, 305-8575 Tsukuba city, Ibaraki, Japan
E-mail: mizukami@md.tsukuba.ac.jp
Tel.: +81-298-533210
Fax: +81-298-533182

M. D. Ikonomovic · E. E. Abrahamson · S. T. DeKosky
Department of Neurology and Alzheimer's Disease Research Center, University of Pittsburgh, 3471 Fifth Avenue, Pittsburgh, PA 15213, USA

Introduction

Over-activation of excitatory amino acid (EAA) receptors leads to excitotoxic neuronal changes that can contribute to neuropathology in Alzheimer's disease (AD) [3, 4, 13, 30]. Excitotoxicity due to excessive EAA receptor stimulation could be countered by compensatory activation of inhibitory neurotransmission. γ-Aminobutyric acid (GABA) is the major inhibitory neurotransmitter in the central nervous system [29] and GABA signaling occurs through two major classes of receptors, the ionotropic $GABA_A$ type, and the metabotropic $GABA_B$ type [20]. Our previous studies demonstrated the relative stability of $GABA_A$ receptor subunits in AD hippocampus [24, 25, 26]. The status of $GABA_B$ receptors, however, remains to be examined.

$GABA_B$ receptor activation increases K^+ conductance, hyperpolarizing postsynaptic sites [19, 32] and inhibiting presynaptic Ca^{2+} conductance, thus suppressing neurotransmitter release and postsynaptic excitatory transmission [31, 37]. $GABA_B$ receptors are composed of at least two heteromers, $GABA_BR1$ (GBR1) and $GABA_BR2$ (GBR2) [17, 18, 36]. Compared to the GBR2, GBR1 immunoreactivity (IR) is more prominent in neuronal soma and proximal dendrites [5],

where pathological material is known to accumulate during the formation of neurofibrillary tangles (NFT) in AD. Therefore, immunohistochemical examination of the GBR1 protein in AD brain allows for the assessment of potential neuronal $GABA_B$ receptor changes relative to the development of NFT pathology. The present study employed immunohistochemical techniques to examine the cellular localization and density of the GBR1 receptor subunit in the hippocampus of 16 elderly subjects at different stages of NFT pathology progression.

Materials and methods

Subjects

Postmortem brain tissue was obtained from 16 elderly subjects: 12 with a clinical diagnosis of AD (mean age ± SD 77.8 ± 13.9 years) and 4 age-matched cognitively normal (CN) control subjects (mean age 73.3 ± 16.5 years). The mean postmortem interval and brain weight of the cases were 5.3 ± 1.9 h and 1,154 ± 138 g, respectively, with no significant difference between AD and CN groups (Table 1). Clinical diagnosis of CN subjects was based on the absence of dementia, determined through retrospective analysis of medical records as well as interviews with family physicians and immediate family members. All AD subjects were participants in a longitudinal research program maintained by the University of Pittsburgh's Alzheimer's Disease Research Center (ADRC). As participants in this program, patients underwent periodic neuropsychological and neurological evaluation. Clinical diagnosis of AD was based on a standardized ADRC evaluation at a Consensus Conference, utilizing DSM-IV [2] and NINCDS/ADRDA [21] criteria. Neuropathological diagnosis was determined by a certified neuropathologist, and was based in part on histological examination of brain tissue sections stained with hematoxylin and eosin, thioflavin-S, and Bielschowsky silver stains. All AD subjects fulfilled CERAD criteria for the diagnosis of "definite" AD [22]. All brains (CN and AD) showed NFT, and dependent on the extent of NFT progression through the entorhinal, hippocampal, and neocortical areas, they were assigned a Braak score, according to neuropathological staging by Braak and Braak [7]. Of the 16 subjects, 4 CN controls were Braak stage I/II with only "mild" hippocampal pathology. Four of the AD patients were in Braak stage III/IV with "moderate" hippocampal pathology, and the remaining eight AD cases were Braak stage V/VI with "severe" hippocampal NFT pathology. Lewy bodies were detected in the cerebral cortex of one moderate case and three severe AD cases, but no Lewy bodies or neurites were detected in the hippocampus of any case. None of the patients included in this study had any confounding neurological or neuropathological disorder, except for isolated old infarcts in the cortex and thalamus of two severe cases (Table 1).

Tissue preparation

Brain tissue was processed according to previously described procedures [24, 26, 27]. The material for this study was obtained from a block of hippocampal tissue cut in the coronal plane at the level of the lateral geniculate body. Tissue was placed in 0.1 M phosphate buffer (PB, pH 7.4) containing 4% paraformaldehyde for 48 h at 4°C, and subsequently cryoprotected in 30% sucrose in PB for several days. Tissue sections for immunohistochemistry were cut at 40 μm on a sliding, freezing microtome. For each case, adjacent sections were stained for Nissl substance to delineate the cytoarchitectural boundaries of hippocampal fields as defined by Duvernoy [10] and Amaral and Insausti [1].

Table 1 Case demographics [*AD* Alzheimer's disease, *CN* cognitively normal controls; *Braak* Braak score (0–VI), *BW* brain weight, *PMI* post mortem interval, Dx diagnosis]

Case	Dx	Age (years)	Gender	BW (g)	PMI (h)	Braak
1	CN	61	F	1,360	8	I/II
2	CN	57	F	1,400	8	I/II
3	CN	87	F	1,120	8	I/II
4	CN	88	F	990	5.5	I/II
5	AD	91	F	1,260	3	III/IV
6	AD	75	M	1,300	7	III/IV
7	AD	81	M	1,150	4	III/IV
8	AD	72	M	1,160	4	III/IV
9	AD	100	F	970	5	V/VI
10	AD	48	M	1,100	8	V/VI
11	AD	86	M	1,330	2	V/VI
12	AD	72	M	1,080	4	V/VI
13	AD	74	M	960	4	V/VI
14	AD	62	M	1,150	4	V/VI
15	AD	84	F	1,070	5	V/VI
16	AD	89	F	1,070	5	V/VI

Immunohistochemistry

Tissue sections were processed free-floating for immunohistochemistry of human GABA receptor subunits as described previously [27, 28], using a polyclonal antibody against the receptor subunit $GABA_BR1$ (GBR1, AB1531; Chemicon, Temecula, CA). The amino acid sequence is common to both the $GABA_BR1a$ and $GABA_BR1b$ receptor isoforms, but this antibody primarily recognizes the $GABA_BR1a$ [38]. The primary antibody was diluted 1:5,000 in TRIS-saline containing 3% goat serum and 0.25% Triton X-100. At least three sections from each case were immunostained for this study. Sections from all cases were processed together to control for variability in the immunohistochemical procedure. As a control for nonspecific staining, sections were incubated with initial incubation media with the primary antibody omitted, and otherwise processed as described. No positive staining was detectable in these control sections. Control sections for each case were used for background correction in optical density (OD) analyses (described below). Double immunolabeling was performed on each case using GBR1 and MC1 antibodies to investigate alterations of GBR1 in neurons undergoing early NFT changes. MC1 (generously provided by Dr. Peter Davies; used at 1:1,000) is a monoclonal antibody that detects early cytoskeletal alterations involving changes in the conformation of the tau molecule [16]. The sequential double-immunolabeling procedure used diaminobenzidine (DAB) as a chromogen to visualize MC1 immunohistochemistry, with subsequent GBR1 immunohistochemistry using DAB and 2.5% nickel ammonium sulfate, yielding homogeneous light brown (DAB) and granular black reaction products (nickel-conjugated DAB). Additional tissue sections were stained using monoclonal 10D5 (1:3,000; Athena Neurosciences, San Francisco, CA) or polyclonal paired helical filament (PHF) tau (1:10,000; DAKO, Carpinteria, CA) antibodies, to visualize amyloid β ($A\beta$) plaques and NFT, respectively.

OD measurements of neuronal GBR1-IR

Quantitative evaluation of the intensity of immunohistochemical reaction in individual pyramidal neurons was performed by OD measurements using an Olympus AHBT-3 light microscope equipped with a SPOT-2 digital video camera (Diagnostic Instruments, San Jose, CA) and public domain image analysis software (NIH Image, Scion, Frederick, MD). All images were obtained at ×40 magnification under constant illumination and exposure conditions. Densitometric analysis was performed as described previously [23, 34]. Briefly, profiles of individual GBR1-immunoreactive neurons with visible nuclei were outlined with a free-hand marquee to obtain a morphometric mask. In three separate non-adjacent sections from each case, ten neurons were randomly selected for measurements in the pyramidal layer of four hippocampal regions (CA1–4) and the subiculum (Sub). The dentate gyrus (DG) granule cell layer was evaluated by randomly choosing three microscopic fields as regions of interests (ROI), in which all neurons were measured collectively, due to their high packing density. The measurement of the relative concentration of GBR1-immunoreactive material in each ROI was obtained as the gray level (GL), related to the OD for the specimen using the following equation:

$$OD = GL_{\text{specimen}} - GL_{\text{background}}$$

where GL_{specimen} is the gray level of the image delineated by the morphometric mask (individual neurons) and $GL_{\text{background}}$ is the gray level of the background reference image (obtained by outlining neuronal layers in sections processed in the absence of primary antibody for each case). Specific staining was defined as the difference in immunostaining intensity between sections incubated with and without the primary antisera.

Values presented are means ± standard deviation (SD). Where appropriate, analysis of variance (ANOVA) was used to make comparisons. If differences were detected by ANOVA, individual groups were compared using the Student-Newman-Keuls test. $P < 0.05$ was accepted as statistically significant for all comparisons.

Cell counts

To compare the relative loss of GBR1-immunoreactive compared to Nissl-labeled pyramidal neurons in CA1 hippocampus, cell counts were performed by randomly selecting ten ×40 microscopic fields on three non-adjacent sections in all cases from each Braak group. All neurons on which the entire soma and initial primary dendrite could be identified were counted within each microscopic field, irrespective of neuronal size (i.e., all pyramidal neurons were counted). The total number of neurons within the entire CA1 field was not calculated; instead, numerical densities of GBR1-immunoreactive and Nissl-labeled neurons were obtained in each case and then calculated as means ± SD for each Braak diagnostic group. Correction for laminar shrinkage was not performed, as shrinkage would affect equally GBR1-IR and Nissl-stained cells counted in adjacent tissue sections. However, it is possible that due to laminar shrinkage the reductions in both GBR-1 and Nissl-positive neurons were underestimated in the Braak stage V/VI group (see discussion). Comparisons across Braak groups were made using ANOVA.

Results

GBR1-IR was detected as black, punctate chromogen precipitate that labeled the soma and proximal dendrites of hippocampal neurons and interneurons. GBR1-IR interneurons were infrequently observed, but were

present in every case; they were either bipolar or multipolar, with fusiform or round cell bodies and thin dendrites (not shown). Unlike pyramidal neurons, GBR1-IR interneurons were located primarily within the strata radiatum and oriens. Neuropil GBR1 immunostaining was not above background levels.

Fig. 1 Photomicrographs showing GBR1 immunohistochemistry in dentate granule cell layer (*GL*) and in CA4 (**A–C**), CA3 (**D–F**), CA2 (**G–I**) and CA1 (**J–L**) subfields of controls that are pathologically "mild" (Braak I/II; **A**, **D**, **G** and **J**), " moderate" AD (Braak III/IV; **B**, **E**, **H**, **K**), and "severe" AD (Braak V/VI; **C**, **F**, **I**, **L**) cases. Compared to mild and severe groups, the overall intensity of neuronal GBR1 immunoreactivity is increased in the moderate cases. In the CA1 subfield of moderate and severe cases, loss of pyramidal cell GBR1 staining is evident (**K**, **L**). This illustrates differences in neuronal GBR1 immunostaining intensity, and is not shown as a representative of differences in numbers of GBR1-immunoreactive neurons across Braak stage groups. The latter numbers are displayed in Table 2 (*GBR1* $GABA_B$ receptor R1 protein, *AD* Alzheimer's disease, *mod* moderate, *sev* severe). *Bar* 100 μm

CN subjects with mild (Braak stage I/II) NFT pathology

In CN subjects, neuronal GBR1-IR was detected in all hippocampal fields, although the intensity of immunostaining differed between fields (Figs. 1A, D, G, J; 2). Within the DG, light GBR1-IR was observed in granule cells (Figs. 1A, 2). In the CA4 field, moderate GBR1-IR was observed in the soma and proximal dendrites of mossy cells (Fig. 1A). In CA3 and CA2, pyramidal cells showed more intense GBR1-IR, particularly in comparison to CA1 field and DG (Figs. 1, 2). In contrast, GBR1-IR of CA1 and Sub pyramidal cells was considerably less intense (Figs. 1J, 2).

AD subjects with moderate (Braak stage III/IV) and severe (Braak stage V–VI) NFT pathology

In hippocampus of moderate AD cases, GBR1-IR increased markedly (Figs. 1, 2) in DG granule cells and

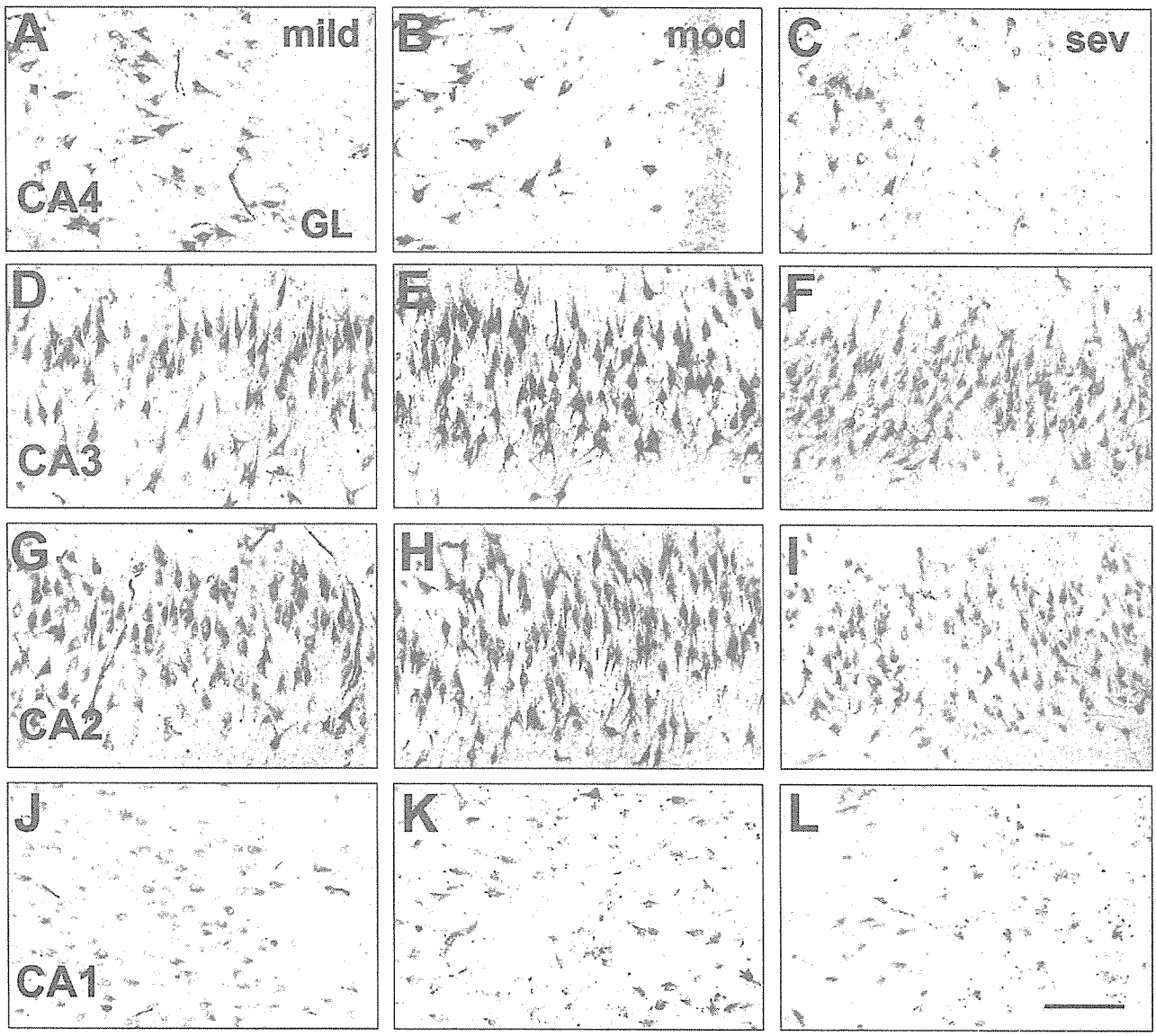

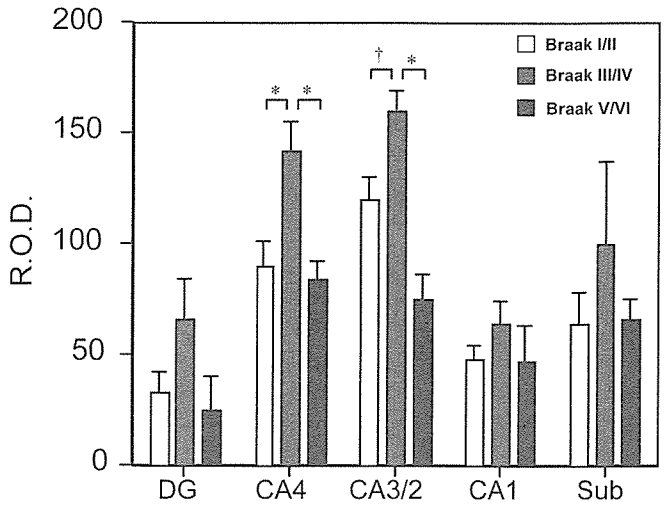

Fig. 2 Bar graph showing R.O.D. measurements of neuronal GBR1 immunostaining intensity in five hippocampal fields in control cases with Braak I/II (mild), and AD patients with Braak III/IV (moderate) or Braak V/VI (severe) pathology. Different patterns can be observed in regions more resistant (DG, CA4, CA3/2) versus those more vulnerable (CA1, Sub) to AD. In cases with an onset of hippocampal NFT pathology (Braak III/IV), significant increases of GBR1 staining intensity are observed in CA4 and CA3/2 regions, while a trend for an increase is seen in DG. *Asterisks*: $P < 0.01$; *dagger*: $P < 0.05$ (*R.O.D.* relative optical density, *DG* dentate gyrus, *CA4*, *CA3/2*, *CA1* hippocampal CA fields, *Sub* subiculum, *NFT* neurofibrillary tangles)

in CA4 and CA3/2 pyramidal cells (Figs. 1B, E, H; 2). In contrast, severe AD cases showed a comparable to decreased cellular GBR1-IR in all hippocampal fields when compared to the mild CN group (Figs. 1C, F, I, L; 2). We next used relative OD (R.O.D.) measurements of neuronal GBR1 immunostaining in individual hippocampal fields to compare GBR1 immunostaining intensity in the three NFT severity groups, and detected significant differences in the CA4 and CA3/2 regions. Moderate AD cases had higher R.O.D. values (Fig. 2) than either mild CN or severe AD groups in CA4 (both $P < 0.01$) or in CA3/2 ($P < 0.05$ and $P < 0.01$). There was a considerable variability in numbers of GBR1-IR and Nissl-stained neurons in the CA1 field of AD cases. Moderate and severe AD cases showed marked loss of GBR1-IR CA1 pyramidal cells compared to the mild CN group (Table 2). Nissl staining of adjacent tissue sections revealed only moderate CA1 pyramidal cell loss across both AD groups, but this is likely an underestimate due to hippocampal atrophy and laminar shrinkage (Table 2; see discussion).

Table 2 Cell counts in the CA1 region (*GBR1* $GABA_B$ receptor R1 protein)

Braak stage	GBR1 positive	Nissl positive
I/II	37.5 ± 14.5	55.8 ± 8.7
III/IV	13.6 ± 9.0*	49.7 ± 12
V/VI	11.3 ± 9.2*	34.2 ± 17.6

*$P < 0.05$ (compared to I/II)

In addition to cellular IR, plaque-like clusters of GBR1-immunoreactive dystrophic neurites were detected in the CA1/Sub (Fig. 3B) and DG molecular layer (not shown) in both moderate and severe AD cases. These clusters were entirely composed of neuritic elements, with no associated neuropil-IR (Fig. 4).

GBR1 and MC1 co-localization in AD hippocampus

Immunostaining with MC1, a marker of early neurofibrillary changes, revealed a differential distribution of MC1-positive neurons in various hippocampal fields of the three groups of cases, consistent with their pathological classification by Braak stages. CN cases showed infrequent MC1-IR cells in the CA1 region, and no labeled neurons in DG, CA3/2 and CA4 (not shown). These CA1 MC1-IR cells did not co-localize GBR1.

In moderate AD cases, MC1-positive neurons were of substantial numbers in CA1/Sub (Fig. 3C), and only infrequent in other fields. In severe AD cases, there was an abundance of MC1-positive cells in CA1/Sub, and substantial numbers in other hippocampal fields. In both AD groups, only a small percentage of CA1/Sub neurons showed co-localization of MC1 and GBR1. In contrast, the CA4 and CA3/2 regions in these cases showed numerous GBR1/MC1 dual-labeled neurons (Fig. 5).

GBR1-positive neuritic plaque-like deposits in AD cases also contained MC1-IR neurites (Fig. 3C). There were no correlations between intensity of neuronal GBR1 immunostaining and distribution of Aβ plaques in hippocampal fields.

Discussion

The present study demonstrates alterations in GBR1-IR during the progression of NFT pathology in the hippocampus of AD subjects. Detection of neuronal GBR1-IR in all hippocampal fields in non-demented cases with only mild neurodegenerative changes is consistent with the results of previous immunohistochemical studies of $GABA_B$ receptors in hippocampus of aged humans [5, 27]. We detected $GABA_B$-IR exclusively in neuronal soma and proximal dendrites. In contrast, Billinton et al. [5] reported that GBR1-IR is also present in the neuropil of the dentate molecular layer and stratum lacunosum-moleculare of the CA fields. Differences in specificity of the antibodies employed in the two studies could account for the discrepancies between the two studies.

Our results indicate that changes in the expression of hippocampal GBR1 subunit correlate with the progression of neuronal degeneration defined by a general assessment of NFT pathology by Braak and Braak [7], as well as by a marker of early NFT changes (MC1). The GBR1 immunostaining was most robust in CA3/2 regions, where it increased markedly in moderate AD

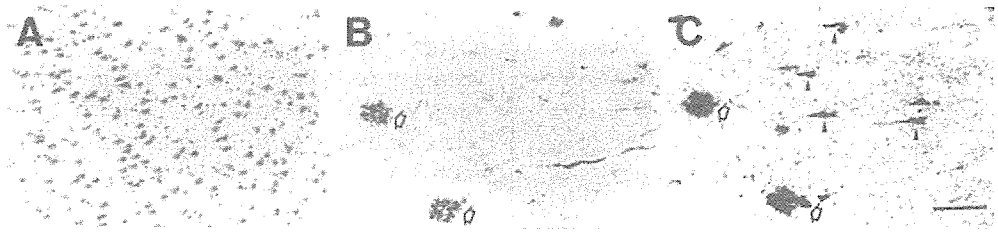

Fig. 3 Photomicrographs of the CA1 field in serial tissue sections, processed for Nissl staining (**A**), GBR1 immunohistochemistry (**B**) and MC1 immunohistochemistry (**C**), from an AD case with moderate (Braak III/IV) NFT pathology. Despite unremarkable neuronal loss (**A**), there is a loss of GBR1 immunoreactivity on pyramidal neurons (**B**) that coincides with appearance of NFTs (**C**, *arrowheads*). Neuritic plaques (*arrowheads*) are both GBR1 positive (**B**) and MC1 positive (**C**). *Bar* 100 μm

(Braak III/IV) cases. In contrast, numbers of GBR1-immunoreactive neurons decreased in the CA1 region in both moderate and severe AD, and no GBR1 up-regulation was observed in these cells. The more pronounced loss of GBR1-immunoreactive compared to Nissl-labeled pyramidal neurons in the CA1 region suggests that GBR1-expressing neurons may be more sensitive to degeneration than CA1 neurons collectively. Notably, the lack of significant loss of Nissl-labeled pyramidal neurons in CA1 in the severe (Braak V/VI) group in the present study differs from that shown in studies employing unbiased stereological techniques [33, 35]. We recognize potential limitations of our non-stereological cell counting method; the latter inconsistency could be due to laminar shrinkage that likely occurs in end-stage AD hippocampus. However, correcting for laminar shrinkage would further reduce the numbers of both GBR1-IR and Nissl-positive CA1 neurons in severe AD cases. While such correction would bring our Nissl cell counting data in closer agreement with previous stereological investigations, we would still observe relatively lower numerical density of GBR1-immunoreactive neurons compared to Nissl-labeled neurons in AD. The CA1 region is particularly vulnerable to AD pathology, while CA3/2 is relatively resistant [11, 12]; thus, elevations in GBR1-IR in CA3/2 pyramidal neurons could reflect a compensatory response to increased excitatory neurotransmission, and render these cells more resistant to excitoxic insults. The $GABA_B$ receptor is known to modulate postsynaptic excitatory transmission [31, 37], and when excitation increases, $GABA_B$-mediated slow inhibition is recruited to offset excessive neuronal excitation [6]. Thus, up-regulation of GBR1 in pyramidal cells could serve to reduce excessive (toxic) stimulation of these cells by increasing inhibitory tone. Thus, transient up-regulation of the GBR1 in pyramidal cells, which occurs at the onset of hippocampal NFT pathology (i.e., Braak stage III/IV), could function to reduce excitotoxic neuronal damage in this region. Previous studies reported that excitotoxicity mediated via calcium-permeable α-amino-3 hydroxy-5-methyl-4-isoazolepropionate (AMPA) and *N*-methyl-D-aspartate (NMDA) types of glutamate receptors may contribute, at least in part, to the development of neurodegenerative changes in the hippocampus [13, 14] as well as in other vulnerable regions [3, 15] of AD brains. In accordance with these studies, we have shown previously that loss of the GluR2 AMPA receptor subunit precedes hippocampal NFT formation [13]. However, it is possible that not only increased excitatory signal, but also reduced GABA compensatory (inhibitory) mechanisms contribute to NFT formation and cell death during the progression of AD. Alternatively, metabolic alterations due to neurofibrillary tangle pathology may impede synthesis of the receptor. Previous studies suggest that GABA receptor subunits can be substantially and selectively affected in AD. For example, radiolabeled ligand binding experiments in the hippocampus [8] and frontal cortex [9] from AD subjects have demonstrated significant reductions in $GABA_B$ receptors, while $GABA_A$ receptors were relatively preserved. Furthermore, $GABA_A$ receptor density was reduced only in stratum pyramidale of CA1 subfield, while reductions in $GABA_B$ receptor density were more extensive [8]. In agreement with these studies, our previous work demonstrated that $GABA_A$ receptor alpha and beta 2/3 protein and beta 2 mRNA signals were well preserved in the DG, even in cases with severe AD pathology, [24, 25, 26]. Collec-

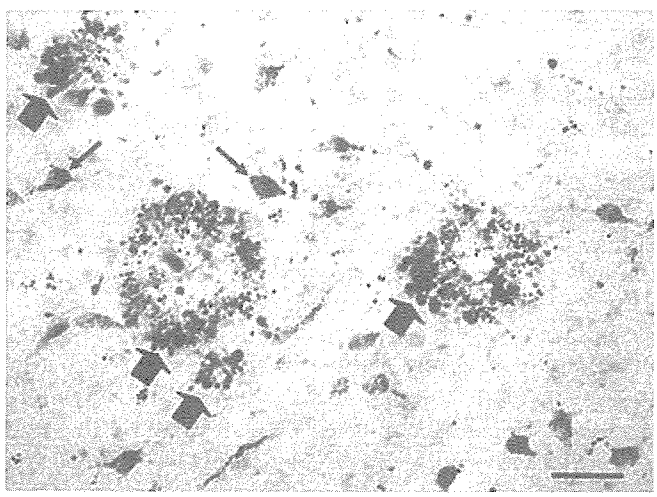

Fig. 4 High-power photomicrograph of three GBR1-immunoreactive plaque-like structures in the CA4. GBR1 immunostaining is present in numerous dystrophic neurites, many of which appear as large bulbous swellings (*large arrows*). Note the punctate GBR1-immunoreactive labeling in nearby neurons (*small arrows*), contrasting the dark uniform labeling seen in neuritic processes. *Bar* 75 μm

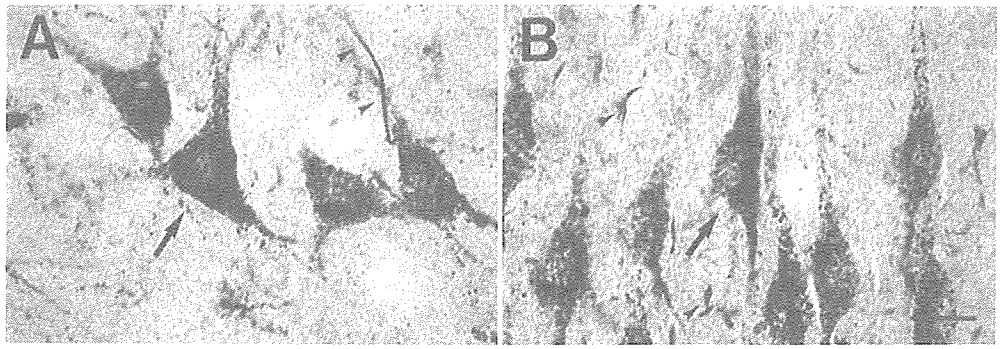

Fig. 5 Photomicrographs showing neuronal double immunolabeling with MC1 (*homogeneous brown*) and GBR1 (*granular purple*) in CA4 (**A**) and CA3 (**B**) subfields of a severe AD case. Co-localization of MC1 and GBR1 is observed in several pyramidal cells (*arrows*). In contrast, MC1-stained neuronal processes and threads (*arrowheads*) are GBR1 negative. *Bar* 20 μm

tively, these results suggest that pathological processes might differentially affect the stability of GABA receptor subunits, with $GABA_B$ being more vulnerable to AD.

We observed that in CA1, an area particularly affected by the development of mature NFT and cell death in AD, neurons expressing an early marker of neurofibrillary changes (MC1) did not co-localize GBR1. In contrast, in the CA3/2 and CA4 regions many of the MC1-immunoreactive neurons also expressed GBR1. Because neurons in the CA1/Sub region are known to develop NFT sooner in the progression of AD than those in any other field in the hippocampus, loss of GBR1 subunits from this cell population might contribute to their propensity to transform into NFT. In contrast, pyramidal neurons from CA3/2 and CA4 regions are resistant to the conversion into NFT, and this might be due to their ability to up-regulate, or sustain, functional GBR1. Thus, early in the course of neurofibrillary change, up-regulation of GBR1 in the CA2/3–4 regions may render these neurons more resistant to the progression of neurofibrillary pathology, whereas in CA1,this compensatory change is either not occurring, or is ineffective. Alternatively, neurons in CA2/3–4 may be more resistant than those in CA1 to the effects of NFT formation, and thereby retain a greater level of GBR1-IR synthesis.

In conclusion, our results indicate that there is a transient increase in GBR1-IR in the hippocampus during the progression of neurofibrillary pathology in the course AD. This potentially compensatory change is not sustainable, as GBR1-IR in severe AD cases is comparable to subjects with only mild NFT pathology. Additionally, there is considerable intersubject variability in AD, with loss of CA1 GBR1-IR in several cases of moderate and severe AD. Thus, changes in $GABA_B$ receptor subunit expression in AD hippocampus could mark a compensatory response to the onset of regional neurodegenerative changes, while loss of such a response might facilitate or be due to further progression of NFT pathology.

Acknowledgements This work was supported by the NIH grant AG05133, and the Research Grant for Longevity Sciences (14C-4) from the Ministry of Health, Labor and Welfare.

References

1. Amaral DG, Insausti R (1990) Hippocampal formation. In: Paxinos G (ed) The human nervous system. Academic Press, New York, pp 711–756
2. American Psychiatric Association (1994) Diagnostic and statistical manual of mental disorders, 4th edn. American Psychiatric Association, Washington, D.C.
3. Armstrong DM, Ikonomovic MD, Sheffield R, Wenthold RJ (1994) AMPA-selective glutamate receptor subtype immunoreactivity in the entorhinal cortex of non-demented elderly and patients with Alzheimer's disease. Brain Res 639:207–216
4. Armstrong DM, Ikonomovic MD, Mizukami K, Mishizin A, Sheffield R, Wolfe BB (1998) Glutamatergic mechanisms in Alzheimer's disease. Advances in Neurodegenerative Disorder: In Marwah J, Teitelbaum H (eds) Alzheimer's and Aging, vol 2, Prominent Press, Scottsdale, pp 71–97
5. Billinton A, Ige AO, Wise A, White JH, Disney GH, Marshall FH, Waldvogel HJ, Faull RLM, Emson PC (2000) $GABA_B$ receptor heterodimer-component localization in human brain. Mol Brain Res 77:111–124
6. Bonard LS (1995) *N*-Methyl-D-aspartate transmission modulates $GABA_B$-mediated inhibition of rat hippocampal pyramidal neurons in vitro. Neuroscience 68:637–643
7. Braak H, Braak E (1991) Neuropathological staging of Alzheimer-related changes. Acta Neuropathol 82:239–259
8. Chu DC, Penney JB Jr, Young AB (1987) Quantitative autoradiography of hippocampal $GABA_B$ and $GABA_A$ receptor changes in Alzheimer's disease. Neurosci Lett 82:246–252
9. Chu DCM, Penny JB, Young AB (1987) Cortical $GABA_B$ and $GABA_A$ receptors in Alzheimer's disease: a quantitative autoradiographic study. Neurology 37:1454–1459
10. Duvernoy HM (1998) The human hippocampus, 2nd edn. Springer, Berlin
11. Flood DG, Guarnaccia M, Coleman PD (1987) Dendritic extent in human CA2–3 hippocampal pyramidal neurons in normal aging and senile dementia. Brain Res 409:88–96
12. Hof PR (1996) Morphology and neurochemical characterics of the vulnerable neurons in brain aging and Alzheimer's disease. Eur Neurol 37:71–81
13. Ikonomovic DM, Mizukami K, Davies P, Hamilton RL, Sheffield R, Armstrong DM (1997) The loss of GluR2(3) immunoreactivity precedes neurofibrillary tangle formation in the entorhinal cortex and hippocampus of Alzheimer brains. J Neuropathol Exp Neurol 56:1018–1027
14. Ikonomovic MD, Mizukami K, Warde D, Sheffield R, Hamilton R, Wenthold RJ, Armstrong DM (1999) Distribution of glutamate receptor subunit NMDAR1 in the hippocampus of normal elderly and patients with Alzheimer's disease. Exp Neurol 160:194–204

15. Ikonomovic MD, Nocera R, Mizukami K, Armstrong DM (2000) Age-related loss of the AMPA receptor subunits GluR2/3 in the human nucleus basalis of Meynert. Exp Neurol 166:363–375
16. Jicha GA, Bozer R, Kazam IG, Davies P (1997) Alz-50 and MC1, a new monoclonal antibody raised to paired helical filaments, recognize confirmational epitopes on recombinant tau. J Neurosci Res 48:128–132
17. Jones KA, borowsky B, Tamm JA, Craig DA, Durkin MM, Dai M, Yao WJ, Johnson M, Gunwaldsen C, huang LY, Tang C, Shen Q, Salon JA, Morse K, Laz T, Smith KE, Nagarathnam D, Noble SA, Branchek TA, Gerald C (1998) $GABA_B$ receptors function as a heterometric assembly of the subunits $GABA_BR1$ and $GABA_BR2$. Nature 396:674–679
18. Kaupmann K, Malitschek B, Schuler V, Heid J, Froestl W, Beck P, mosbacher J, bichoff S, Kulik A, Shigemoto R, Karschin A, Bettler B (1998) $GABA_B$-receptor subtypes assemble into functional heterometric complexs. Nature 396:683–687
19. Luscher C, Jan LY, Stoffel M, Malenka RC, Nicoll RA (1997) G protein-coupled inwardly rectifying K^+ channels (GIRKs) mediate postsynaptic but not presynaptic transmitter actions in hippocampal neurons. Neuron 19:687–695
20. Macdonald RL, Olsen RW (1994) $GABA_A$ receptor channels. Annu Rev Neurosci17:569–602
21. McKhann G, Drachman D, Folstein M, Katzman, R, Price D, Stadlan EM (1984) Clinical diagnosis of Alzheimer's disease: report of Health and Human Services Task Force on Alzheimer's disease. Neurology 34:939–944
22. Mirra SS, Heyman A, McKeel D, Sumi SM, Crain BJ, Brownlee LM, Vogel FS, Hughes JP, van Belle G, Berg L (1991) The consortium to establish a registry for Alzheimer's disease (CERAD). Part II. Standardization of the neuropathologic assessment of Alzheimer's disease. Neurology 41:479–486
23. Mize RR (1994) Quantitative image analysis for immunocytochemistry and in situ hybridization. J Neurosci Methods 54:219–237
24. Mizukami K, Ikonomovic MD, Grayson DR, Rubin RT, Warde D, Sheffield R, Hamilton RL, Davies P, Armstrong DM (1997) Immunohistochemical study of $GABA_A$ receptor $\beta 2/3$ subunits in the hippocampal formation of aged brains with Alzheimer-related neuropathologic changes. Exp Neurol 147:333–345
25. Mizukami K, Grayson DR, Ikonomovic MD, Sheffield R, Armstrong DM (1998) $GABA_A$ receptor $\beta 2$ and $\beta 3$ subunits mRNA in the hippocampal formation of aged human brain with Alzheimer-related neuropathology. Mol Brain Res 56:268–272
26. Mizukami K, Ikonomovic MD, Grayson DR, Sheffield R, Armstrong DM (1998) Immunohistochemical study of $GABA_A$ receptor $\alpha 1$ subunit in the hippocampal formation of aged brains with Alzheimer-related neuropathologic changes. Brain Res 799:148–155
27. Mizukami K, Sasaki M, Ishikawa M, Iwakiri M, Hidaka S, Shiraishi H, Iritani S (2000) Immunohistochemical localization of $GABA_B$ receptor in the hippocampus of subjects with schizophrenia. Neurosci Lett 283:101–104
28. Mizukami K, Ishikawa M, Hidaka S, Iwakiri M, Sasaki M, Iritani S (2002) Immunohistochemical localization of GABAB receptor in the entorhinal cortex and inferior temporal cortex of schizophrenic brain. Prog Neuropsychopharmacol Biol Psychiatry 26:393–396
29. Möhler H, Benke D, Benson J, Lüscher B, Rudolph U, Fritschy JM (1997) Diversity in structure, pharmacology, and regulation of $GABA_A$ receptors. In: Enna SJ, Bowery NG (eds) GABA receptors, 2nd edn. Humana Press, Clifton, pp 11–36
30. Palmer AM, Gershon S (1990) Is the neuronal basis of Alzheimer's disease cholinergic or glutamatergic? FASEB J 4:2745–2752
31. Pfrieger FW, Gottmann K, Lux HD (1994) Kinetics of $GABA_B$ receptor-mediated inhibition of calcium currents and excitatory synaptic transmission in hippocampal neurons in vitro. Neuron 12:97–107
32. Premkumar LS, Gage PW (1994) Potassium channels activated by $GABA_B$ agonists and serotonin in cultured hippocampal neurons. J Neurophysiol 71: 2570–2575
33. Rössler M, Zarski R, Bohl J, Ohm TG (2002) Stage-dependent and sector-specific neuronal loss in hippocampus during Alzheimer's disease. Acta Neuropathol 103:363–369
34. Smolen AJ (1990) Image analytic techniques for quantification of immunohistochemical staining in the nervous system. In: Conn PM (ed) Methods in Neurosciences, vol 3. Academic Press, New York, pp 208–229
35. West MJ (1993). Regionally specific loss of neurons in the aging human hippocampus. Neurobiol Aging 14:287–293
36. White JH, Wise A, Main MJ, Green A, Fraser NJ, Disney GH, Barnes AA, Emson P, Foord SM, Marshall FH (1998) Heterodimerization is required for the formation of a functional $GABA_B$ receptor. Nature 396:679–682
37. Wu LG, Saggau P (1995) $GABA_B$ receptor-mediated presynaptic inhibition in guinea-pig hippocampus is caused by reduction of presynaptic Ca^{2+} influx. J Physiol 485:649–657
38. Yung KKL, Ng TKY, Wong CKC (1999) Subpopulations of neurons in the rat neotriatum display $GABA_BR1$ receptor immunoreactivity. Brain Res 830:345–352

ELSEVIER

Clinical Neurophysiology 116 (2005) 729–737

www.elsevier.com/locate/clinph

EEG filtering based on blind source separation (BSS) for early detection of Alzheimer's disease

Andrzej Cichocki[a,b,*], Sergei L. Shishkin[a], Toshimitsu Musha[c], Zbigniew Leonowicz[a,d], Takashi Asada[e], Takayoshi Kurachi[c]

[a]*Laboratory for Advanced Brain Signal Processing, RIKEN Brain Science Institute, 2-1 Hirosawa, Wako-shi, Saitama 351-0198, Japan*
[b]*Warsaw University of Technology, Warsaw, Poland*
[c]*Brain Functions Laboratory Inc., KSP Building E211, Sakado, Takatsu Kawasaki, Kanagawa, 213-0012, Japan*
[d]*Wroclaw University of Technology, Wroclaw, Poland*
[e]*Department of Neuropsychiatry, Tsukuba University, Tennoudai, Tsukuba-shi, 305-8575, Japan*

Accepted 16 September 2004
Available online 28 October 2004

Abstract

Objective: Development of an EEG preprocessing technique for improvement of detection of Alzheimer's disease (AD). The technique is based on filtering of EEG data using blind source separation (BSS) and projection of components which are possibly sensitive to cortical neuronal impairment found in early stages of AD.

Methods: Artifact-free 20 s intervals of raw resting EEG recordings from 22 patients with Mild Cognitive Impairment (MCI) who later proceeded to AD and 38 age-matched normal controls were decomposed into spatio-temporally decorrelated components using BSS algorithm 'AMUSE'. Filtered EEG was obtained by back projection of components with the highest linear predictability. Relative power of filtered data in delta, theta, alpha 1, alpha 2, beta 1, and beta 2 bands were processed with Linear Discriminant Analysis (LDA).

Results: Preprocessing improved the percentage of correctly classified patients and controls computed with jack-knifing cross-validation from 59 to 73% and from 76 to 84%, correspondingly.

Conclusions: The proposed approach can significantly improve the sensitivity and specificity of EEG based diagnosis.

Significance: Filtering based on BSS can improve the performance of the existing EEG approaches to early diagnosis of Alzheimer's disease. It may also have potential for improvement of EEG classification in other clinical areas or fundamental research. The developed method is quite general and flexible, allowing for various extensions and improvements.

Keywords: Alzheimer's disease; Diagnosis; EEG; Blind Source Separation; AMUSE; Filtering

1. Introduction

Alzheimer's disease (AD) is one of the most frequent disorders among the elderly population (Jeong, 2004; Petersen, 2003). Recent studies have demonstrated that AD has a presymptomatic phase, likely lasting years, during which neuronal degeneration is occurring but clinical symptoms do not yet appear. This makes preclinical discrimination between people who will and will not ultimately develop AD critical for early treatment of the disease which could prevent or at least slow down the onset of clinical manifestations of disease (Blennow and Hampel, 2003; DeKosky and Marek, 2003; Rapoport, 2000; Wagner, 2000). Moreover, early diagnostic tools could significantly facilitate the development of drugs for the treatment at the early stage of AD: without preclinical diagnosis, many times more subjects (potential patients with huge percentage of those who actually would never develop AD) should be involved for testing of these drugs (DeKosky and Marek, 2003). A diagnostic method should be relatively inexpensive to make possible screening of many individuals who are at risk of developing this dangerous disease

* Corresponding author. Tel.: +81 48 467 9668; fax: +81 48 467 9686.
E-mail address: cia@brain.riken.jp (A. Cichocki).

1388-2457/$30.00 © 2004 Published by Elsevier Ireland Ltd. on behalf of International Federation of Clinical Neurophysiology.
doi:10.1016/j.clinph.2004.09.017

(DeKosky and Marek, 2003). The electroencephalogram (EEG) is one of the most promising candidates to become such a method.

To date, many signal processing techniques were applied for revealing pathological changes in EEG associated with AD (see Jeong, 2004, for review). For example, combination of linear and nonlinear measures improved the classification accuracy of AD versus normal subjects up to 92% (Pritchard et al., 1994). Using principal component analysis (PCA) as a postprocessing tool for compressing linear and nonlinear EEG features over channels and age as a moderator variable in a study with rigorous validation procedure (jack-knifing), Besthorn et al. (1997) obtained 89% correct classification. However, high classification accuracy was obtained for patients who already developed serious cognitive impairment (e.g. Mini Mental State Examination (MMSE) score was 11.5 ± 7.9 in the study of Besthorn et al. (1997)).

Finding a method for identification of patients who have no clinical signs of AD at the moment of EEG registration but later progress to AD is the main challenge in this field. The studies of this kind are very rare. Huang et al. (2000) obtained 87% classification accuracy for discrimination between patients with mild cognitive impairment (MCI) who later progressed and not progressed to AD, however, without reporting the use of cross-validation. Musha and co-authors demonstrated, in a computer simulation, that local cortical neuronal impairment should lead to lower dipolarity (goodness-of-fit for dipole localizations) of alpha EEG frequency components (Hara et al., 1999), and then, based on these results, developed a technique for estimation of cortical impairment in AD using a single index of dipolarity (Musha et al., 2002). Alpha dipolarity was able to differentiate MCI patients who showed no clinical signs of AD at the time when EEG was recorded but developed AD later, as diagnosed in the follow-up, from normal controls with high probability; it also correlated with the degree of cortical neuronal impairment, estimated by SPECT (Musha et al., 2002).

However, in spite of all of the achievements made in the above cited studies, the problem of preclinical diagnosis of AD using EEG is not yet solved and further improvement of the methodology is necessary.

The main idea of this paper can be formulated as 'filtering based on Blind Source Separation (BSS)', that is, filtering of EEG by selection of most relevant components followed by reconstruction of the relevant part (subspace) of EEG signal using back projection of only these components. We propose a preprocessing technique based on this idea for improving EEG-based AD diagnosis (possibly useful also in other fields of EEG analysis). Its usefulness was evaluated in combination with standard procedures, namely the linear discriminant analysis (LDA) applied to spectral power in several frequency bands. To make comparison clear and fair, we used only most reliable but simple procedures. However, more sophisticated analysis based on recent advances in techniques for EEG processing and data classification may provide, in combination with proposed preprocessing, further significant improvement of early AD diagnosis, and some relevant emerging techniques will be mentioned in Discussion.

2. Methods

2.1. Blind source separation filtering for EEG classification

Intuitively, one can expect that some hidden components of such a complex signal like EEG can be more sensitive to Alzheimer's disease and the related disorders than others. These more sensitive components can be considered as useful 'signal', and the other components of EEG as 'noise' or 'unwanted signals'. Improving the 'signal-to-noise ratio' by filtering off the 'noise' could enhance the performance of subsequent feature extraction and data classification. Blind Source Separation (BSS) algorithms (see Cichocki and Amari, 2003, for extensive review) can be used for the purpose of such filtering.

BSS, in its application to EEG analysis, assume that EEG signal is composed of a finite number of components (signals from the brain and other sources), $s(t) = [s_1(t),\ldots,s_n(t)]^T$. Here t is a discrete time index, n is the number of components and $[\ldots]^T$ means transpose of row vector. Components are mixed through unknown linear mixing process (described by $n \times n$ mixing matrix $\mathbf{A}$), and n sensors (EEG electrodes) record the mixed signals $\mathbf{x}(t) = \mathbf{A}\mathbf{s}(t)$. Each of the components changes in time, but has a fixed weight for each channel. BSS algorithm finds an unmixing (separating) $n \times n$ matrix $\mathbf{W}$ consisting of coefficients with which the electrode signals should be taken to form, by summation, the estimated components: $\mathbf{y}(t) = \mathbf{W}\mathbf{x}(t)$. (In more general case, the number of components can be not equal to the number of sensors.) The entries of the estimated mixing matrix $\hat{\mathbf{A}} = \mathbf{W}^{-1}$ are components' weights in the mixing process; in other words, they indicate how strongly each electrode picks up each of individual components. *Back projection* of some selected components $\mathbf{x}_r(t) = \mathbf{W}^{-1}\mathbf{y}_r(t)$ (where $\mathbf{x}_r(t)$ is a vector of reconstructed sensor signals and $\mathbf{y}_r(t)$ is the vector obtained from the vector $\mathbf{y}(t)$ after removal of all the undesirable components (i.e. by replacing them with zeros)) allows us to filter the EEG data.

In strict sense, BSS means estimation of true (original) sources, though exactly the same procedure can be used for separation of two or more subspaces of the signal without estimation of true sources. One procedure currently becoming popular in EEG analysis is removing artifact-related BSS components and back projection of components originating from brain (e.g. Jung et al., 2000; Joyce et al., 2004; Vorobyov and Cichocki, 2002). In this procedure, components of brain origin are not required to be separated from each other exactly, because they are mixed again by

back projection after removing artifact-related components. But by the same procedure we can filter off the 'noise' also in wider sense, improving the relative amount of any types of useful information in the signal. Specifically, we can try to increase the relative amount of signal content related to AD (i.e. to improve signal to noise ratio — SNR).

Finding the rules or fundamental principles for identification of *relevant and irrelevant components* is critical for the proposed approach and, in general, may require extensive studies. In the case of removing artifact-related components, such components typically can be easily identified by visual inspection, but in more general case exact discrimination of relevant and non-relevant components is more difficult. In this paper we attempt to differentiate clusters or subspaces of components with similar properties or features. For the purposes of EEG classification the estimation of individual components corresponding to separate and meaningful brain sources is not required, unlike in other applications of BSS to EEG processing (including its most popular variant, Independent Component Analysis (ICA)). The use of clusters of components is especially beneficial when the data from different subjects are compared: similarity between individual components in different subjects is usually low, while subspaces formed by similar components are more likely to be sufficiently overlapped. Differentiation of subspaces with high and low amount of diagnostically useful information can be made easier if components are separated and sorted according to some criteria which, at least to some extent, correlate with the diagnostic value of components. BSS algorithm 'AMUSE', in our opinion, can be relevant for this task.

2.2. AMUSE algorithm and its properties

AMUSE (Cichocki and Amari, 2003; Szupiluk and Cichocki, 2001; Tong et al., 1991, 1993)) is a BSS algorithm which arranges components not only in the order of decreasing variance (that is typical for the use of singular value decomposition (SVD) which is implemented within the algorithm), but also in the order of their decreased linear predictability. Low values for both characteristics can be specific for many of EEG components related to high frequency artifacts, especially electromyographic signal (which cannot be sufficiently removed by usual filtering in frequency domain, see Goncharova et al., 2003). Thus, a first attempt of selection of diagnostically important components can be made by removing a range of components separated with AMUSE (below referred to as 'AMUSE components') with the lowest linear predictability. Automatic sorting of components by this algorithm makes it possible to do this simply by removing components with indices higher than some chosen value.

AMUSE algorithm belongs to the group of second-order-statistics spatio-temporal decorrelation (SOS-STD) BSS algorithms. It provides similar decomposition as the well known and popular SOBI algorithms (Belouchrani et al., 1997; Tang et al., 2002). AMUSE algorithm uses simple principles that the estimated components should be spatio-temporally decorrelated and be less complex (i.e. have better linear predictability) than any mixture of those sources. The components are ordered according to decreasing values of singular values of a time-delayed covariance matrix. As in Principal Component Analysis (PCA) and unlike in many ICA algorithms, all components estimated by AMUSE are uniquely defined (i.e. any run of algorithms on the same data will always produce the same components) and consistently ranked. Fig. 1 illustrates typical components obtained by decomposing EEG using AMUSE algorithm.

AMUSE algorithm can be considered as two consecutive PCAs: first, PCA is applied to input data; second, PCA (SVD) is applied to the time-delayed covariance matrix of the output of previous stage. In the first step standard or robust prewhitening (sphering) is applied as a linear transformation $\mathbf{z}(t)=\mathbf{Q}\mathbf{x}(t)$, where $\mathbf{Q}=\mathbf{R}_x^{-\frac{1}{2}}$ of the standard covariance matrix $\mathbf{R}_x=E\{\mathbf{x}(t)\mathbf{x}^T(t)\}$ and $\mathbf{x}(t)$ is a vector of observed data for time instant t. Next, SVD is applied to a time-delayed covariance matrix of pre-whitened data: $\mathbf{R}_z=E\{\mathbf{z}(t)\mathbf{z}^T(t-1)\}=\mathbf{U}\mathbf{S}\mathbf{V}^T$, where $\mathbf{S}$ is a diagonal matrix with decreasing singular values and $\mathbf{U}$, $\mathbf{V}$ are matrices of eigenvectors. Then, an unmixing matrix is estimated as $\mathbf{W}=\hat{\mathbf{A}}^{-1}=\mathbf{U}^T\mathbf{Q}$ or $\hat{\mathbf{A}}=\mathbf{Q}^T\mathbf{U}$.

AMUSE algorithm is much faster than the vast majority of BSS algorithms (its processing speed is mainly defined by the PCA processing within it) and is very easy to use, because no parameters are required. It is implemented as a part of package 'ICALAB for signal processing' (Cichocki et al., online) freely available online and can be called also from the current version of EEGLAB toolbox (Delorme and Makeig, 2004) (which is freely available online at http://www.sccn.ucsd.edu/eeglab/) if both toolboxes are installed.

2.3. Subjects and EEG recording

We used EEG recordings collected in the previous study (Musha et al., 2002). In that study, patients who complained only for memory impairment, but had no apparent loss in general cognitive, behavioral, or functional status, were recruited. Fifty-three patients of this group met the following criteria for Mild Cognitive Impairment (MCI): MMSE score 24 or higher, Clinical Dementia Rating (CDR) scale score of 0.5 with memory performance less than one standard deviation below the normal reference (Wechsler Logical Memory Scale and Paired Associates Learning subtests, IV and VII, ≤ 9 (Wechsler, 1987), and/or ≤ 5 on the 30 min delayed recall of the Rey-Osterreith figure test (Hodges, 1993)). These patients were followed clinically for 12–18 months. Twenty-five of them developed probable or possible AD according to NINDS-ADRDA criteria (McKhann et al., 1984). Normal age-matched controls were recruited from family members of the patients

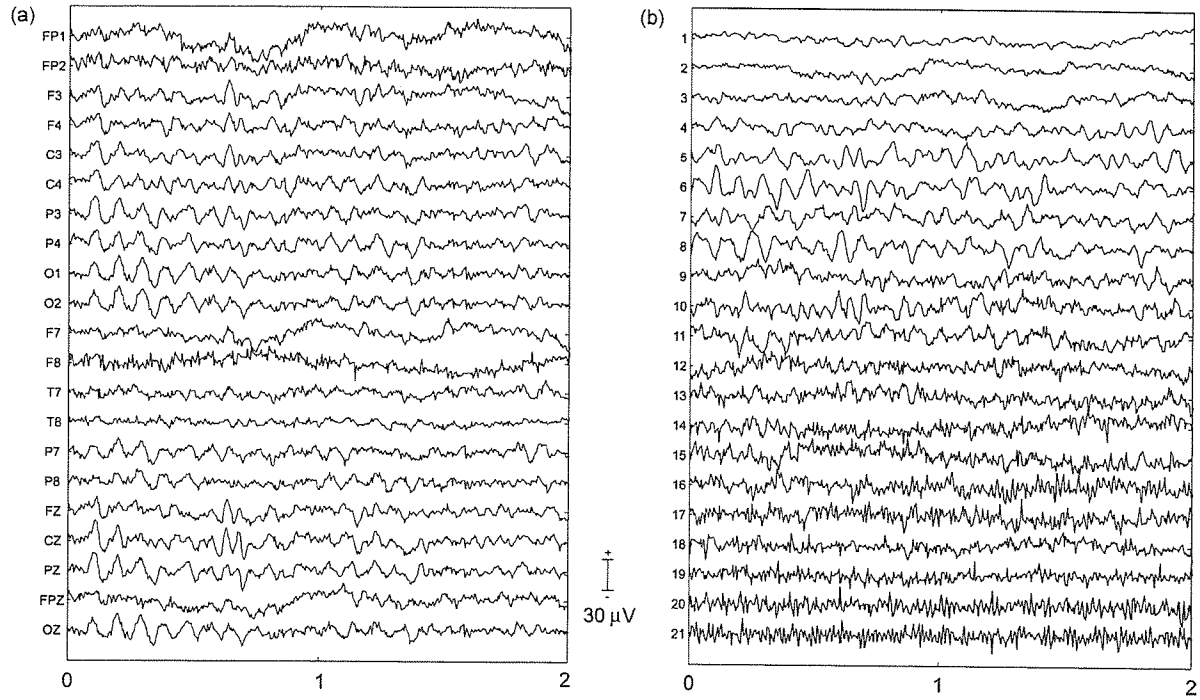

Fig. 1. Example of raw EEG (a) and its components separated with AMUSE algorithm (b) for a patient with MCI who later progressed to AD (MildAD002). AMUSE was applied to 20 s artifact-free interval of EEG, but only 2 s are shown. The scale for the components is arbitrary but linear. Note that the components are automatically ordered according to decreasing linear predictability (increasing complexity).

(mainly spouses) participated in the study as control group. Both patients and controls underwent general medical, neurological, psychiatric, and neuroimaging (SPECT, CT and MRI) investigation for making the diagnosis more precise.

EEG was recorded within 1 month after entering the study from all patients and controls, but only EEG recorded from the patients who progressed to AD ($n=25$; below: MCI group) and age-matched controls ($n=56$) was used for the analysis. No patient or control subject received psychotropic medication at the period when EEG was recorded. Mean MMSE score was 26 ± 1.8 in MCI group and 28.5 ± 1.6 in control group; age 71.9 ± 10.2 and 71.7 ± 8.3, respectively. EEG recording was done in an awake resting state with eyes closed, under vigilance control. Ag/AgCl electrodes (disks of diameter 8 mm) were placed on 21 sites according to 10–20 international system, with the reference electrode on the right ear-lobe. EEG was recorded with Biotop 6R12 (NEC San-ei, Tokyo, Japan) using analog filtering bandpass 0.5–250 Hz and sampling rate 200 Hz.

2.4. EEG data analysis

All computations were done using MATLAB (The MathWorks, Inc.). EEGLAB (Delorme and Makeig, 2004) was used for visual analysis of EEG recordings, and AMUSE algorithm implemented in ICALAB (Cichocki et al., online) was used for BSS processing.

Out of the EEG database described above (from the study of Musha et al., 2002), we selected 25 MCI patients (later progressed to AD) and 47 age-matched controls who had relatively little artifacts. Their EEGs were visually inspected by an experienced EEG researcher and the first continuous artifact-free 20 s interval of each recording was chosen for the analysis. Due to the lack of such interval in some recordings, the number of patients and controls were reduced to 22 and 38, correspondingly. The reason for selecting artifact-free intervals was that most of the artifacts produced amplifier blocking (saturation) due to its low amplitude range, which lead to strongly nonlinear distortion of the signal. AMUSE, as most of BSS methods, assumes a linear model of summation of source signals, and amplifier blocking should be excluded from the data.

Each EEG was decomposed into 21 decorrelated components by BSS algorithm AMUSE (see above). Some of the components (see Results) were selected for back projection, which formed preprocessed ('AMUSE filtered') EEG data. Spectral analysis based on Fast Fourier Transform (Welch method, Hanning 1 s window, 2 s epochs overlapped by 0.5 s) was applied to raw data, to the components and to the projections of selected components. Relative spectral powers were computed by dividing the power in delta (1.5–3.5 Hz), theta (3.5–7.5 Hz), alpha 1 (7.5–9.5 Hz), alpha 2 (9.5–12.5 Hz), beta 1 (12.5–17.5 Hz) and beta 2 (17.5–25 Hz) bands by the power in 1.5–25 Hz band. These values were normalized for better fitting

the normal distribution using the transformation $\ln(x/(1-x))$, where x is the relative spectral power (Gasser et al., 1982). To reduce the number of variables used for classification, we averaged band power values over all 21 channels.

Linear discriminant analysis (LDA) (using publicly available software for both linear classical and robust discriminant analysis, by Croux and Dehon, 2001) was used for discriminating MCI and control groups on the basis of log-transformed relative spectral power in the six frequency bands, averaged over channels. To improve validation of the classification results, discriminant analysis was applied in combination with jack-knifing, a procedure which typically produces lower discrimination rate than, e.g. cross-validation based on using part of a sample for learning and other part for classification, but is statistically more correct and enables increased reproducibility in other samples (Besthorn et al., 1997). Jack-knifing means that each case is classified using individual discriminant function trained with all cases except this one. Results of this procedure was used for computing sensitivity (the number of MCI subjects who were classified as MCI divided by the number of all subjects in MCI group) and specificity (the number of normal subjects who were classified as normal divided by number of all normal subjects).

3. Results

Averaged power spectra of each AMUSE component for patients and control subjects are presented in Fig. 2. As expected, components with lower indices (corresponding to higher linear predictability) had higher relative power at lower frequencies, while components with higher indices had higher relative power at highest frequencies. What is especially important is that the difference between patients and control subjects was clearer in the components with lower indices (i.e. components with highest linear predictability and highest variance of their projections). Thus, in further analysis we used combination of components with lowest indices.

To estimate how many components with highest linear predictability provides optimal classification rate, we applied LDA without jack-knifing (the latter requires much more computation time) to all projected components with indices from 1 to 2, from 1 to 3 and so on. Overall misclassification rate was computed each time by applying obtained discriminant function to the same 60 subjects (22 patients + 38 controls). Results are presented in Fig. 3. The best classification was obtained for projection of the first five components (with indices from 1 to 5); however, performance was also high when the number of components

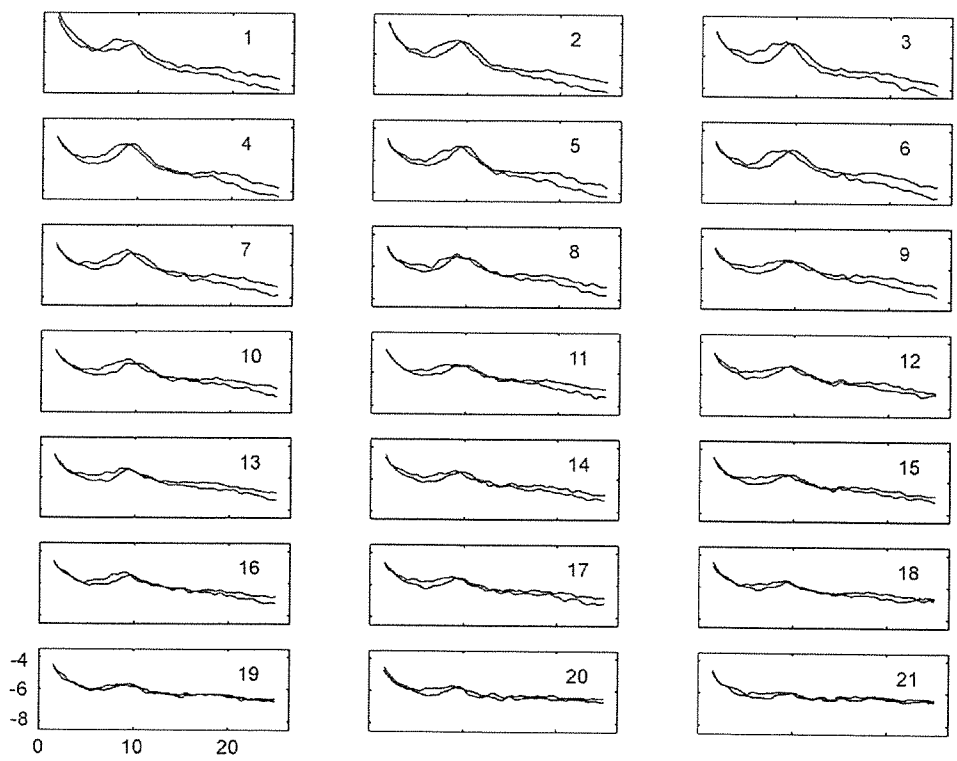

Fig. 2. Averaged power spectra of AMUSE components 1–21. x-axis: frequency, Hz. y-axis: transformed relative spectral power. Relative spectral power was obtained by dividing the absolute values in each frequency bin by total power in the range 1.5–25 Hz. Before averaging, the power values were normalized using transformation $\log(x/(1-x))$ (negative values appear because of this transformation). Red: MCI patients later progressed to AD ($n=22$). Black: control subjects ($n=38$).

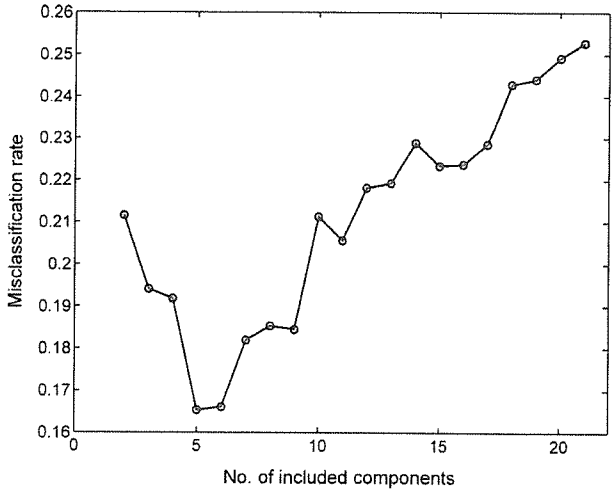

Fig. 3. LDA approximate (computed without cross-validation) misclassification rate for different number of projected components. Only components with highest linear predictability were used, thus, data points correspond to the following combinations of components: 1,2; 1–3; 1–4;...1–20; 1–21.

was in a rather wide range between 3 and 9. Thus, the method appeared to be robust in respect to the number of selected components.

Classification with jack-knifing procedure was applied to projections of several combinations of components, including 1–5 which appeared to be optimal according to Fig. 3. As follows from Table 1, results of classification were better if preprocessing included selection of AMUSE components with lower indices (1–5, 1–7, 1–10), comparing to raw data. When components with higher indices (6–21, 8–21, 11–21) were selected in preprocessing, the results were worse than in the case of raw data. Best results were obtained with components 1–5 and 1–7 (improvement by 14% over the raw data for classification of MCI and by 8% for control subjects), while components 11–21 gave the worst results. More detailed classification results for two combinations of components (1–5 and 1–10) and for the raw data, presented as Relative Operating Characteristic (ROC) curves in Fig. 4, confirm that use of components 1–10 only slightly improved the classification (Fig. 4(a)), while improvement of classification with components 1–5 over raw data was substantial (Fig. 4(b)). Best classification performance after preprocessing using 1–5 components was obtained in the range of approximately 0.6–0.8 for sensitivity and 0.7–0.9 for specificity. Selection of components with high indices was clearly not good for classification: for components 11–21 classification performance was almost at random level (Fig. 4(a)).

Table 1
Number of subjects who were correctly and incorrectly classified by discriminant analysis applied to relative power in six frequency bands after selection and back projection of certain AMUSE components (AMUSE filtering). Results were obtained using jack-knifing

AMUSE components selected in preprocessing	Misclassified		Correctly classified %		
	MCI $n=22$	Controls $n=38$	MCI $n=22$	Controls $n=38$	All $n=60$
No preprocessing	9	9	59	76	70
Components 1–5	**6**	**6**	**73**	**84**	**80**
Components 1–7	**6**	**6**	**73**	**84**	**80**
Components 1–10	6	9	73	76	75
Components 6–21	9	11	59	71	67
Components 8–21	9	11	59	71	67
Components 11–21	**12**	**12**	**45**	**68**	**60**

4. Discussion

With EEG preprocessing proposed in this paper, we obtained 80% rate of correct classification (Table 1) for MCI using only 20 s artifact-free interval of EEG recording from each patient or control subject. While groups of patients and controls were relatively small (22 and 38, correspondingly), it should be noted that the classification performance was estimated using the rigorous jack-knifing cross-validation procedure, which reduce the risk of overstating the results. The jack-knifing procedure was applied only to LDA but not to approximate optimization of the choice of components for back projection. Optimization of the choice of components was made for the whole dataset on the basis of components' spectra and preliminary run of LDA. Nevertheless, Figs. 2 and 3 suggest that the dependence of the difference between patients' and controls' spectra on component index and dependence of LDA results on the number of selected components were systematic; thus, it is unlikely that we simply picked up some random variations in LDA performance dependent on details of preprocessing and that improvement of LDA performance by preprocessing with the same parameters will be not reproducible in other groups of patients and controls.

The procedure of selection of artifact-free EEG intervals used in this study could introduce some bias in absolute values of discrimination results, because it was done by only one expert, and this expert did know to which group each EEG belongs. In fact, the proportion of the EEG recordings which were not analyzed due to the lack of a sufficiently long artifact-free interval was different in the groups of patients (12%) and controls (19%), and this difference was in the direction which can be expected if the criteria for selecting the analyzed interval were more strict for control group. This difference could be a result of random variations, and it should be noted that most of artifacts were easily identifiable (due to low amplifier range, any high amplitude artifact led to amplifier saturation), so it was rather unlikely that the subjective bias could strongly

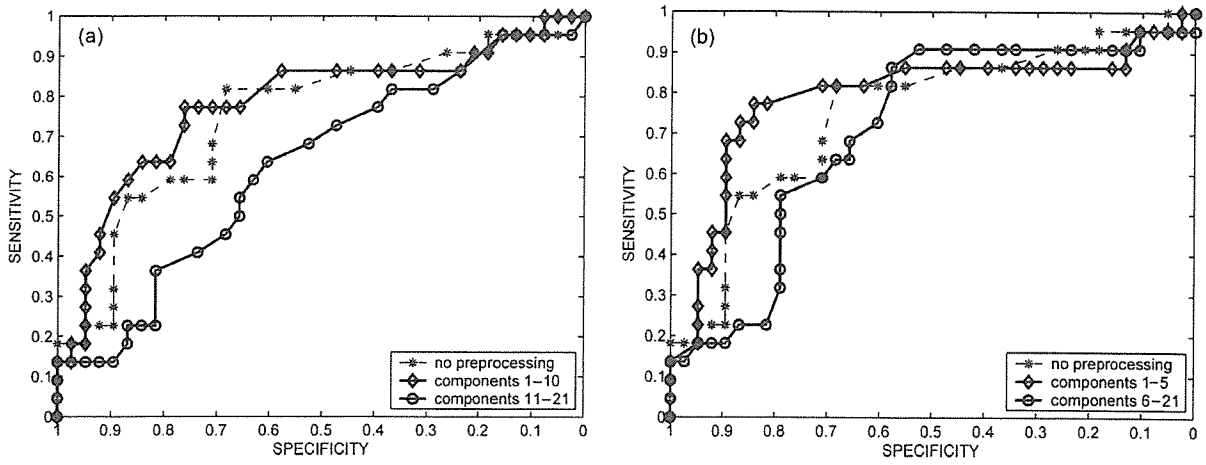

Fig. 4. Relative Operating Characteristic (ROC) curves obtained using jack-knifing for classification of MCI patients later progressed to AD (n=22) versus normal controls (n=38). LDA was applied to relative power in six EEG frequency bands. Comparison between data without preprocessing and data after selection and back projection of certain AMUSE components (AMUSE filtering). (a) Selection of first 10 components, compared to the rest of components and no preprocessing. (b) Selection of first five components, compared to the rest of components and no preprocessing.

influence the results. However, we cannot guarantee that the use of subjective criteria for selection of artifact free intervals did not affect classification results at all, and it is difficult to predict whether the obtained high values of specificity and sensitivity can be reproduced in other studies. We would like to emphasize, nevertheless, that our main claim is that the proposed preprocessing method increases the performance *relatively* to the level obtained without its use. This tendency could not be altered by subjective bias in search for artifact-free intervals.

We do not discuss here to which physiologically meaningful brain sources AMUSE components can correspond, because they can be a mixture of activity from many physical sources in the brain. This is clearly not critical for improving of EEG classification. The improvement of classification after AMUSE filtering comparing to non-preprocessed EEG data was probably caused by higher difference between patients' and controls' spectra in the selected components than in the non-used (filtered off) components. Spectra computed for AMUSE components separated by BSS algorithm AMUSE (Fig. 2) demonstrate that the difference between patients and controls decreased with the index of component. Interestingly, this effect is visible at the same time in several frequency ranges: in theta range, where patients had an increase of relative power; in alpha range, where shift of the peak to slower frequencies was observed in patients; and in beta range, where relative power was lower for patients. All these differences in spectral power are typically found between AD patients and normal subjects. Spectra of components with the highest indices showed almost no difference between patients and controls, and it was not surprising that the performance of classification based on back projection of only these components was close to random level (Fig. 4(a), components 11–21). Thus, AMUSE components with higher indices can be considered as mainly representing 'noise' which makes difficult, in processing of raw EEG, to detect diagnostically important changes in characteristics of 'signal'. Note that 'signal' and 'noise' here are not labels for signal from brain sources and for artifacts: we refer to the 'signal' only as to diagnostically important (significant) part (subspace) of raw EEG signal, and to 'noise' as to the diagnostically not important part (non-significant subspace). AMUSE filtering, i.e. extraction of part of EEG reach with 'signal' by using only 'best' (here, most useful for diagnosis) components for back projection, naturally leads to the improvement of 'signal-to-noise ratio' and, as a result, to the improvement of EEG classification.

A BSS-based approach to improvement of signal-to-noise ratio in MEG signal by defining and removing noise subspace was already developed (Kawakatsu, 2003). More simple and already rather widely used technique is removing EEG and MEG artifact-related components with BSS using visual or automatic identification of such components one by one after decomposition (e.g. Jung et al., 2000). However, since in many kinds of EEG and MEG studies the goal is to extract the brain signal in possibly less distorted form, the existing techniques are limited to remove only such part of raw signal, which contain no or almost no components of brain origin but rather external artifacts and noise. In EEG classification tasks, such as diagnosis or Brain-Computer Interface (BCI), preserving the original signal is less important, noise can be defined not only as artifacts but also as any part of the signal which do not contribute to the difference between the classes of EEG which should be differentiated, and larger subspace with high percentage of such 'noise' can be removed. The existing techniques can only identify, by some a priori known characteristics, noise components (Barbati et al., 2004; Jung et al., 2000; Kawakatsu, 2003)

and some very specific diagnostically important components (epileptic spike separation: e.g. Kobayashi et al., 2002). Xu et al. (2004) recently suggested using a subspace approach for differentiating between task-related EEG patterns in BCI. They selected several ICA components related to P300 according to the a priori knowledge of P300 spatio-temporal pattern and reconstructed a clear P300 peak using back projection of these components. Like in the case of epileptic spikes, the components in this case were easily identifiable.

In a general case, however, significant and non-significant components are not easily identifiable. The task becomes especially challenging if EEG components from different subjects should be compared, because the sets of components produced by BSS in different subjects usually differ dramatically. In our approach, we rank components using some empirical rule, such as their linear predictability, and select those where difference between the pathological and normal EEG is most differentiated. This made possible to achieve substantial improvement in the discrimination between MCI patients who later progressed to AD and normal age-matched controls. To our best knowledge, no study till now investigated the application of BSS/ICA methods as preprocessing tools with possible application for AD diagnosis.

Dividing of components into two groups (or subspaces) as below or above some component's index (in the case of ranking) or using a threshold for some index computed for each component is not the only way. One may try to divide the sets of components at more than one level and, e.g. remove not only components with highest indices but also with the lowest indices. As one may suppose from Fig. 1(b) (example of individual data), the first two components could represent, to rather high extent, artifacts (roving eye movements). Fig. 2, however, shows that components #1 and #2 substantially differed between groups. We made an attempt to exclude 1 or 2 first components from the analysis and this, in fact, led to slightly lower discrimination results. However, it is possible that for other data (for example, including high amplitude low frequency artifacts) or other processing techniques dividing the set of components on more than one level could be beneficial.

Not only spectral but also other EEG features, such as measures of synchronization between channels, can be investigated for the possibility of improving contrast between pathological and normal data using the presented approach. Several studies indicated that synchronization between different brain areas is sensitive to AD. Such results were obtained for quite different techniques, including coherence (e.g. Adler et al., 2003; Jelic et al., 1996; Locatelli et al., 1998; Wada et al., 1998), mutual information (Jeong et al., 2001) and synchronization likelihood (a new measure combining estimation of linear and nonlinear coupling) (Stam et al., 2003). One may hypothesize that EEG components can be divided into two parts, one of which represents signal subspace with lower (or stronger) synchronization among some cortical areas in AD relative to normal EEG, and another one represents signal subspace which synchronization characteristics are not related to the disease. In this case, the general approach described in this paper also could appear to be useful. One may probably try to apply it also in the case of using nonlinear measures (see review in Jeong, 2004) or in combination with other advanced approaches.

There is obviously room for improvement and extension of the proposed method both in ranking and selection of optimal (significant) components, apparatus and post-processing to perform classification task. Especially, we can apply a wide variety of BSS methods, i.e. instead of the applied and investigated second order statistics spatio-temporal decorrelation, we can exploit other new types of BSS algorithms, such as higher order statistic ICA, sparse component analysis or smooth component analysis with a suitably ordered and ranked components. Furthermore, instead of standard LDA we can use more sensitive and robust methods, such as neural networks or support vector machine (SVM) classifiers. Classification can be probably strongly improved by supplementing the set of spectral power values which we used with much different indices, such as alpha dipolarity, a new index depending on prevalence local vs. distributed sources of EEG alpha activity, which was shown to be very sensitive to AD-related cortical impairment (Musha et al., 2002). Additional attractive but still open issue is that using the proposed approach, we can not only detect but also measure in consistent way the progression of AD and influence of medications. The proposed method can also be potentially useful and effective tool for differential diagnosis of AD from other types of dementia, and possibly for diagnosis of other diseases. Other areas of EEG analysis can be also possible field for the application of our preprocessing technique. For these purposes, more studies would be needed to asses of the impact of the proposed enhancement/filtering procedures on the EEG signal of interest.

References

Adler G, Brassen S, Jajcevic A. EEG coherence in Alzheimer's dementia. J Neural Transm 2003;110(9):1051–8.

Barbati G, Porcaro C, Zappasodi F, Rossini PM, Tecchio F. Optimization of an independent component analysis approach for artifact identification and removal in magnetoencephalographic signals. Clin Neurophysiol 2004;115(5):1220–32.

Belouchrani A, Abed-Meraim K, Cardoso JF, Moulines E. A blind source separation technique using second order statistics. IEEE Trans Signal Process 1997;45(2):434–44.

Besthorn C, Zerfass R, Geiger-Kabisch C, Sattel H, Daniel S, Schreiter-Gasser U, et al. Discrimination of Alzheimer's disease and normal aging by EEG data. Electroencephalogr Clin Neurophysiol 1997; 103(2):241–8.

Blennow K, Hampel H. CSF markers for incipient Alzheimer's disease. Lancet Neurol 2003;2(10):605–13.

Cichocki A, Amari S. Adaptive blind signal and image processing: learning algorithms and applications. New York, NY: Wiley; 2003.

Cichocki A, Amari S, Siwek K, Tanaka T, et al. ICALAB toolboxes. [Available online at http://www.bsp.brain.riken.jp/ICALAB]

Croux C, Dehon C. Software package for robust discriminant analysis; 2001. [http://www.econ.kuleuven.ac.be/public/NDBAE06/software/DA/matlab.htm]

DeKosky ST, Marek K. Looking backward to move forward: early detection of neurodegenerative disorders. Science 2003;302(5646): 830–4.

Delorme A, Makeig S. EEGLAB: an open source toolbox for analysis of single-trial EEG dynamics including independent component analysis. J Neurosci Methods 2004;134(1):9–21.

Gasser T, Bacher P, Mocks J. Transformations towards the normal distribution of broad band spectral parameters of the EEG. Electroencephalogr Clin Neurophysiol 1982;53(1):119–24.

Goncharova II, McFarland DJ, Vaughan TM, Wolpaw JR. EMG contamination of EEG: spectral and topographical characteristics. Clin Neurophysiol 2003;114(9):1580–93.

Hara J, Shankle WR, Musha T. Cortical atrophy in Alzheimer's disease unmasks electrically silent sulci and lowers EEG dipolarity. IEEE Trans Biomed Eng 1999;46(8):905–10.

Hodges JR. Cognitive assessment for clinicians. Oxford: Oxford Medical Publications; 1993 p. 197–228.

Huang C, Wahlund L, Dierks T, Julin P, Winblad B, Jelic V. Discrimination of Alzheimer's disease and mild cognitive impairment by equivalent EEG sources: a cross-sectional and longitudinal study. Clin Neurophysiol 2000;111(11):1961–7.

Jelic V, Shigeta M, Julin P, Almkvist O, Winblad B, Wahlund LO. Quantitative electroencephalography power and coherence in Alzheimer's disease and mild cognitive impairment. Dementia 1996;7(6): 314–23.

Jeong J. EEG dynamics in patients with Alzheimer's disease. Clin Neurophysiol 2004;115(7):1490–505.

Jeong J, Gore JC, Peterson BS. Mutual information analysis of the EEG in patients with Alzheimer's disease. Clin Neurophysiol 2001;112(5): 827–35.

Joyce CA, Gorodnitsky IF, Kutas M. Automatic removal of eye movement and blink artifacts from EEG data using blind component separation. Psychophysiology 2004;41(2):313–25.

Jung TP, Makeig S, Westerfield M, Townsend J, Courchesne E, Sejnowski TJ. Removal of eye activity artifacts from visual event-related potentials in normal and clinical subjects. Clin Neurophysiol 2000;111(10):1745–58.

Kawakatsu M. Application of ICA to MEG noise reduction. Fourth international symposium on independent component analysis and blind signal separation (ICA2003), Nara, Japan; April 1–4, 2003, p. 535–41.

Kobayashi K, Akiyama T, Nakahori T, Yoshinaga H, Gotman J. Systematic source estimation of spikes by a combination of independent component analysis and RAP-MUSIC. II: preliminary clinical application. Clin Neurophysiol 2002;113(5):725–34.

Locatelli T, Cursi M, Liberati D, Franceschi M, Comi G. EEG coherence in Alzheimer's disease. Electroencephalogr Clin Neurophysiol 1998; 106(3):229–37.

McKhann G, Drachman D, Folstein M, Katzman R, Price D, Stadlan EM. Clinical diagnosis of Alzheimer's disease: report of the NINCDS-ADRDA Work Group under the auspices of Department of Health and Human Services Task Force on Alzheimer's Disease. Neurology 1984; 34(7):939–44.

Musha T, Asada T, Yamashita F, Kinoshita T, Chen Z, Matsuda H, et al. A new EEG method for estimating cortical neuronal impairment that is sensitive to early stage Alzheimer's disease. Clin Neurophysiol 2002; 113(7):1052–8.

Petersen RC, editor. Mild cognitive impairment: aging to Alzheimer's Disease. New York: Oxford University Press. 2003.

Pritchard WS, Duke DW, Coburn KL, Moore NC, Tucker KA, Jann MW, et al. EEG-based, neural-net predictive classification of Alzheimer's disease versus control subjects is augmented by non-linear EEG measures. Electroencephalogr Clin Neurophysiol 1994; 91(2):118–30.

Rapoport SI. Functional brain imaging to identify affected subjects genetically at risk for Alzheimer's disease. Proc Natl Acad Sci USA 2000;97(11):5696–8.

Stam CJ, van der Made Y, Pijnenburg YA, Scheltens P. EEG synchronization in mild cognitive impairment and Alzheimer's disease. Acta Neurol Scand 2003;108(2):90–6.

Szupiluk R, Cichocki A. Blind signal separation using second order statistics. Proceedings of SPETO; 2001, p. 485–8.

Tang AC, Pearlmutter BA, Malaszenko NA, Phung DB. Independent components of magnetoencephalography: single-trial response onset time estimation. NeuroImage 2002;17:1773–89.

Tong L, Soon V, Huang YF, Liu R. Indeterminacy and identifiability of blind identification. IEEE Trans CAS 1991;38:499–509.

Tong L, Inouye Y, Liu R. Waveform-preserving blind estimation of multiple independent sources. IEEE Trans Signal Process 1993;41(7): 2461–70.

Vorobyov S, Cichocki A. Blind noise reduction for multisensory signals using ICA and subspace filtering, with application to EEG analysis. Biol Cybern 2002;86(4):293–303.

Wada Y, Nanbu Y, Koshino Y, Yamaguchi N, Hashimoto T. Reduced interhemispheric EEG coherence in Alzheimer disease: analysis during rest and photic stimulation. Alzheimer Dis Assoc Disord 1998;12(3): 175–81.

Wagner AD. Early detection of Alzheimer's disease: an fMRI marker for people at risk. Nat Neurosci 2000;3(10):973–4.

Wechsler D. Wechsler memory scale: revised manual. San Antonio, TX: Psychological Corp.; 1987.

Xu N, Gao X, Hong B, Miao X, Gao S, Yang F. BCI Competition 2003—Data set IIb: enhancing P300 wave detection using ICA-based subspace projections for BCI applications. IEEE Trans Biomed Eng 2004;51(6): 1067–72.

Available online at www.sciencedirect.com
SCIENCE DIRECT®
Neuroscience Letters 379 (2005) 149–151
Neuroscience Letters
www.elsevier.com/locate/neulet

Association study of the chemokine, CXC motif, ligand 1 (CXCL1) gene with sporadic Alzheimer's disease in a Japanese population

Yoshiko Tamura[a,1], Yuji Sakasegawa[a,1], Kazuya Omi[a,b], Hitaru Kishida[a,c], Takashi Asada[d], Hideo Kimura[a], Katsushi Tokunaga[b], Naomi S. Hachiya[a], Kiyotoshi Kaneko[a], Hirohiko Hohjoh[a,*]

[a] *National Center of Neurology and Psychiatry, National Institute of Neuroscience, 4-1-1 Ogawahigashi, Kodaira, Tokyo 187-8502, Japan*
[b] *Department of Human Genetics, Graduate School of Medicine, The University of Tokyo, 7-3-1 Hongo, Bunkyo-ku, Tokyo 113-0033, Japan*
[c] *Department of Neurology, Yokohama City University School of Medicine, Yokohama 236-0004, Japan*
[d] *Department of Neuropsychiatry, Institute of Clinical Medicine, University of Tsukuba, Tsukuba 305-8577, Japan*

Received 25 November 2004; received in revised form 21 December 2004; accepted 22 December 2004

Abstract

Inflammation is profoundly involved in the development of Alzheimer's disease (AD) and other neurodegenerative diseases. Chemokine, CXC motif, ligand 1 (CXCL1; or GRO1) is an inflammatory cytokine and appears to be implicated in the pathogenesis of AD. It is of interest and importance to see if the *CXCL1* gene, mapped on chromosome 4q12–q13, has potential for conferring the predisposition to AD. Here we report on an association study of the *CXCL1* gene with sporadic AD patients in a Japanese population; three single nucleotide polymorphisms (SNPs) in the *CXCL1* locus were investigated in 103 AD patients and 130 healthy individuals. The results indicate that neither genotype frequencies nor allele frequencies of the examined SNPs attained statistical significance even after being stratified by the presence or absence of the *Apolipoprotein E* ε4 allele. Therefore, the data presented here suggests that the *CXCL1* gene could not be associated with the susceptibility to AD in a Japanese population.

Keywords: Alzheimer' disease; Chemokine; CXC motif, ligand 1 (CXCL1); Single nucleotide polymorphisms (SNPs); Association study

Alzheimer's disease (AD) is a progressive neurodegenerative disorder of the elderly, and characterized by accumulation of neurofibrillary tangles and amyloid deposition resulting in the formation of senile plaques in the brain. Sporadic AD other than familial AD appears to be a multifactorial disorder in which both genetic and environmental factors are involved [2]. A genetic factor strongly associated with sporadic AD has been found in the *Apolipoprotein E* (*APOE*) gene: the *APOE ε4* allele increases the predisposition to AD [10,12,13]. It is likely that other genetic factors besides *APOE ε4* could participate in developing AD, and it is of importance and necessary to determine such genetic factors conferring the predisposition to AD.

Chemokines are inflammatory cytokines which have multiple functions in the immune system, and also have effects on cells of the central nervous system [1,3,4,7–9,15–17]. It appears that inflammation is implicated in the pathogeneses of various neurodegenerative disorders including AD [9,14–17]. Previous study suggested that chemokine, CXC motif, ligand 1 (CXCL1; or GRO1) could work as a potent trigger for the ERK1/2 and PI-3 kinase pathway and induce hypermethylation of the tau protein in mouse primary cortical neurons, and also that the immunoreactivity for CXCL1 increased in a subpopulation of neurons in some AD brains [14]. It was further suggested that a chemokine receptor for CXCL1, CXCR2, was expressed on neurons and was strongly upregulated in a subpopulation of senile plaques in AD [9,15].

* Corresponding author. Tel.: +81 42 342 2711x5176; fax: +81 42 346 1748.
E-mail address: hohjohh@ncnp.go.jp (H. Hohjoh).
[1] These authors contributed equally to this work.

0304-3940/$ – see front matter © 2005 Elsevier Ireland Ltd. All rights reserved.
doi:10.1016/j.neulet.2004.12.056

Table 1
Genotype and allele frequencies of the SNPs in the *CXCL1* locus

SNP name (position[a])		Patients ($n = 103$)	Controls ($n = 130$)	P	OR (95% CI)
rs3117602	Genotype frequency				
(75,199,137)	C/C	90 (87.4%)	107 (82.3%)	0.43	1.0
	C/A	13 (12.6%)	22 (16.9%)		0.7 (0.3–1.5)
	A/A	0 (0%)	1 (0.8%)		–
	Allele frequency				
	C allele	93.7%	90.7%	0.25	
	A allele	6.3%	9.3%		
rs4074	Genotype frequency				
(75,202,395)	G/G	26 (25.2%)	31 (23.8%)	0.95	1.0
	G/A	55 (53.4%)	72 (55.4%)		0.9 (0.45–1.7)
	A/A	22 (21.4%)	27 (20.8%)		1.0 (0.4–2.0)
	Allele frequency				
	G allele	51.9%	51.6%	0.93	
	A allele	48.1%	48.4%		
rs1429638	Genotype frequency				
(75,204,181)	C/C	46 (44.7%)	59 (45.4%)	0.92	1.0
	C/A	51 (49.5%)	65 (50.0%)		1.0 (0.6–1.7)
	A/A	6 (5.8%)	6 (4.6%)		1.3 (0.4–4.2)
	Allele frequency				
	C allele	69.4%	70.2%	0.82	
	A allele	30.6%	29.8%		

[a] The nucleotide positions are based on the numbering used in the NCBI public location.

These observations lead to the possibility that the *CXCL1* gene could confer the predisposition to sporadic AD, i.e., it may be a genetic risk factor for AD, and stimulate our interest in studying if there is any association between the *CXCL1* gene and AD.

In this study, we investigated three single nucleotide polymorphisms (SNPs) around the *CXCL1* locus mapped on 4q12–q13 in sporadic AD patients and healthy individuals. The subjects were all Japanese: 103 patients with AD (47 men and 56 women; mean age of onset, 70.7 years old) were diagnosed by meeting the National Institute of Neurological and communicative Disorders and Stroke and The Alzheimer's Disease and Related Dementias Association criteria (NINCDS-ADRDA) [11], and 130 unrelated healthy individuals (57 men and 73 women; mean age, 70.9 years old) were examined as controls. Peripheral blood samples were obtained and subjected to isolation of genomic DNA with standard protocols. For a high-throughput analysis, allelic discrimination assay with commercially available Assays-on-Demand SNP Genotyping products (Applied Biosystems) was carried out in 25 μl of 1 × TaqMan Universal PCR Master Mix (Applied Biosystems) containing ~10 ng of genomic DNA and 1.25 μl of an Assays-on-Demand SNP Genotyping product (Applied Biosystems) by using the Applied Biosystems 7300 Real Time PCR System (Applied Biosystems) according the manufacture's instructions. The Assays-on-Demand SNP Genotyping products used (the Assay ID numbers; public ID numbers) were as follows: C_9761059_10; rs3117602 (intergenic SNP), C_11820472_1; rs4074 (intron3 SNP), C_2042711_10; rs1429638 (intergenic SNP). The SNPs cover the *CXCL1* gene and the physical distances between rs3117602 and rs4074 SNPs and between rs4074 and rs1429638 SNPs are approximately 3.3 and 1.8 kb long, respectively. After SNP typing, statistical analyses of the data were carried out using SNPAlyse (DYNACOM, Yokohama, Japan). The presence of Hardy-Weinberg equilibrium was examined by χ^2-test for goodness of fit. Allele distributions between the patients and controls were examined by χ^2-test for independence. As for haplotype analysis, haplotype frequencies and linkage disequilibrium parameters were estimated on the basis of an expectation-maximization algorithm [5]. Case–control haplotype analyses were carried out by using the permutation method to obtain the empirical significance [6]. Each haplotype was tested for association by grouping all other haplotypes together and applying χ^2-test with 1 d.f. P values were estimated on the basis of 10,000 replications.

Table 1 shows the results of the SNP typing in the AD patients and healthy controls. The SNPs examined in this study revealed no significant differences in their genotype frequencies, allele frequencies and allele carrier frequencies between the patients and healthy controls. In addition, none of the polymorphisms in each group deviated from expectations based on Hardy-Weinberg equilibrium at a significance level of 0.01. Accordingly, although there was a limitation in the number of the subjects used in this study, i.e., the numbers of the patients and controls used were small; the typing data suggested that the *CXCL1* gene could not be a major risk factor conferring the susceptibility to AD at least. We further examined allelic associations (haplotypes) among the rs3117602, rs4074 and rs1429638 SNPs. As a result, strong

Table 2
Estimated haplotypes and their frequencies

Haplotypes[a]	Patients (n = 103), HF (%)	Controls (n = 130), HF (%)	P
C–G–C	51.9	50.5	0.75
C–A–A	29.4	28.9	0.66
C–A–C	12.3	11.4	0.75
A–A–C	5.2	7.5	0.32

HF: haplotype frequency.
[a] Estimated haplotypes with the rs3117602, rs4074 and rs1429638 SNPs are indicated and the haplotypes with 5% or more of their frequencies are shown.

allelic associations (haplotypes) among the SNPs were detectable in either the healthy controls or AD patients (Table 2); but, the estimated haplotype frequencies resulted in no significant difference between the patients and controls. We must add that further analyses stratified by either the presence or absence of the *APOE ε4* allele resulted in no statistical significance, although the difference in the frequency of the *APOE ε4* allele alone between the patients and controls attained statistical significance ($P = 0.0079$). Taking all the data together, it is suggested that the *CXCL1* gene is not associated with the susceptibility to sporadic AD. Since inflammation appears to be implicated in the development of AD, it is conceivable that the *CXCL1* gene could contribute to only inflammatory response in the course of the development of AD, but not participate in the pathogenesis of AD as a genetic factor conferring the predisposition to AD.

Acknowledgments

We would like to thank Dr. N. Minami for providing the DNA samples of patients. This work was supported by the Millennium Project of Alzheimer's Disease in Japan.

References

[1] A. Bajetto, R. Bonavia, S. Barbero, T. Florio, G. Schettini, Chemokines and their receptors in the central nervous system, Front Neuroendocrinol. 22 (2001) 147–184.
[2] D. Blacker, L. Bertram, A.J. Saunders, T.J. Moscarillo, M.S. Albert, H. Wiener, R.T. Perry, J.S. Collins, L.E. Harrell, R.C. Go, A. Mahoney, T. Beaty, M.D. Fallin, D. Avramopoulos, G.A. Chase, M.F. Folstein, M.G. McInnis, S.S. Bassett, K.J. Doheny, E.W. Pugh, R.E. Tanzi, Results of a high-resolution genome screen of 437 Alzheimer's disease families, Hum. Mol. Genet. 12 (2003) 23–32.
[3] R. Bonavia, A. Bajetto, S. Barbero, P. Pirani, T. Florio, G. Schettini, Chemokines and their receptors in the CNS: expression of CXCL12/SDF-1 and CXCR4 and their role in astrocyte proliferation, Toxicol. Lett. 139 (2003) 181–189.
[4] C.M. Coughlan, C.M. McManus, M. Sharron, Z. Gao, D. Murphy, S. Jaffer, W. Choe, W. Chen, J. Hesselgesser, H. Gaylord, A. Kalyuzhny, V.M. Lee, B. Wolf, R.W. Doms, D.L. Kolson, Expression of multiple functional chemokine receptors and monocyte chemoattractant protein-1 in human neurons, Neuroscience 97 (2000) 591–600.
[5] L. Excoffier, M. Slatkin, Maximum-likelihood estimation of molecular haplotype frequencies in a diploid population, Mol. Biol. Evol. 12 (1995) 921–927.
[6] D. Fallin, A. Cohen, L. Essioux, I. Chumakov, M. Blumenfeld, D. Cohen, N.J. Schork, Genetic analysis of case/control data using estimated haplotype frequencies: application to APOE locus variation and Alzheimer's disease, Genome Res. 11 (2001) 143–151.
[7] J.K. Harrison, C.M. Barber, K.R. Lynch, cDNA cloning of a G-protein-coupled receptor expressed in rat spinal cord and brain related to chemokine receptors, Neurosci. Lett. 169 (1994) 85–89.
[8] J.K. Harrison, Y. Jiang, S. Chen, Y. Xia, D. Maciejewski, R.K. McNamara, W.J. Streit, M.N. Salafranca, S. Adhikari, D.A. Thompson, P. Botti, K.B. Bacon, L. Feng, Role for neuronally derived fractalkine in mediating interactions between neurons and CX3CR1-expressing microglia, Proc. Natl. Acad. Sci. U.S.A. 95 (1998) 10896–10901.
[9] R. Horuk, A.W. Martin, Z. Wang, L. Schweitzer, A. Gerassimides, H. Guo, Z. Lu, J. Hesselgesser, H.D. Perez, J. Kim, J. Parker, T.J. Hadley, S.C. Peiper, Expression of chemokine receptors by subsets of neurons in the central nervous system, J. Immunol. 158 (1997) 2882–2890.
[10] S.M. Laws, E. Hone, S. Gandy, R.N. Martins, Expanding the association between the APOE gene and the risk of Alzheimer's disease: possible roles for APOE promoter polymorphisms and alterations in APOE transcription, J. Neurochem. 84 (2003) 1215–1236.
[11] G. McKhann, D. Drachman, M. Folstein, R. Katzman, D. Price, E.M. Stadlan, Clinical diagnosis of Alzheimer's disease: report of the NINCDS-ADRDA Work Group under the auspices of Department of Health and Human Services Task Force on Alzheimer's Disease, Neurology 34 (1984) 939–944.
[12] M. Michikawa, K. Yanagisawa, Apolipoprotein E4 induces neuronal cell death under conditions of suppressed de novo cholesterol synthesis, J. Neurosci. Res. 54 (1998) 58–67.
[13] A.M. Saunders, W.J. Strittmatter, D. Schmechel, P.H. George-Hyslop, M.A. Pericak-Vance, S.H. Joo, B.L. Rosi, J.F. Gusella, D.R. Crapper-MacLachlan, M.J. Alberts, et al., Association of apolipoprotein E allele epsilon 4 with late-onset familial and sporadic Alzheimer's disease, Neurology 43 (1993) 1467–1472.
[14] M. Xia, B.T. Hyman, GROalpha/KC a chemokine receptor CXCR2 ligand, can be a potent trigger for neuronal ERK1/2 and PI-3 kinase pathways and for tau hyperphosphorylation—a role in Alzheimer's disease? J. Neuroimmunol. 122 (2002) 55–64.
[15] M. Xia, S. Qin, M. McNamara, C. Mackay, B.T. Hyman, Interleukin-8 receptor B immunoreactivity in brain and neuritic plaques of Alzheimer's disease, Am. J. Pathol. 150 (1997) 1267–1274.
[16] M.Q. Xia, B.J. Bacskai, R.B. Knowles, S.X. Qin, B.T. Hyman, Expression of the chemokine receptor CXCR3 on neurons and the elevated expression of its ligand IP-10 in reactive astrocytes: in vitro ERK1/2 activation and role in Alzheimer's disease, J. Neuroimmunol. 108 (2000) 227–235.
[17] M.Q. Xia, B.T. Hyman, Chemokines/chemokine receptors in the central nervous system and Alzheimer's disease, J. Neurovirol. 5 (1999) 32–41.